Nanomedicine: Nanotechnology, Biology, and Medicine
12 (2016) 909–919

nanomedicine
Nanotechnology, Biology, and Medicine

nanomedjournal.com

Superparamagnetic iron-oxide nanoparticles mPEG350– and mPEG2000-coated: cell uptake and biocompatibility evaluation

Adny H. Silva, PhD[a], Enio Lima Jr. PhD[b], Marcelo Vasquez Mansilla, PhD[b], Roberto D. Zysler, PhD[b], Horacio Troiani, PhD[b], Mary Luz Mojica Pisciotti, MSc[b], Claudriana Locatelli, PhD[c], Juan C. Benech, PhD[d], Natalia Oddone, MSc[d], Vinícius C. Zoldan, PhD[e], Evelyn Winter, PhD[a], André A. Pasa, PhD[e], Tânia B. Creczynski-Pasa, PhD[a,*]

[a]*Departamento de Ciências Farmacêuticas, Universidade Federal de Santa Catarina, Florianópolis, SC, Brazil*
[b]*Div. Resonancias Magneticas, Centro Atómico Bariloche/CONICET, S. C., Bariloche, Argentina*
[c]*Curso de Farmácia, Universidade do Oeste de Santa Catarina, Videira, SC, Brazil*
[d]*Inst. de Investigaciones Biológicas Clemente Estable, Montevideo, Uruguay*
[e]*Departamento de Física, Universidade Federal de Santa Catarina, Florianópolis, SC, Brazil*

Received 4 August 2015; accepted 14 December 2015

Abstract

Superparamagnetic iron oxide nanoparticles (SPIONS) were synthesized by thermal decomposition of an organometallic precursor at high temperature and coated with a bi-layer composed of oleic acid and methoxy-polyethylene glycol-phospholipid. The formulations were named SPION-PEG350 and SPION-PEG2000. Transmission electron microscopy, X-ray diffraction and magnetic measurements show that the SPIONs are near-spherical, well-crystalline, and have high saturation magnetization and susceptibility. FTIR spectroscopy identifies the presence of oleic acid and of the conjugates mPEG for each sample. *In vitro* biocompatibility of SPIONS was investigated using three cell lines; up to 100 μg/ml SPION-PEG350 showed non-toxicity, while SPION-PEG2000 showed no signal of toxicity even up to 200 μg/ml. The uptake of SPIONS was detected using magnetization measurement, confocal and atomic force microscopy. SPION-PEG2000 presented the highest internalization capacity, which should be correlated with the mPEG chain size. The *in vivo* results suggested that SPION-PEG2000 administration in mice triggered liver and kidney injury.

Key words: Superparamagnetic iron-oxide nanoparticles (SPIONS); Uptake; Biocompatibility; *In vitro*; *In vivo*

Superparamagnetic iron-oxide nanoparticles (SPIONS) are being extensively investigated as a promising tool for cell target drug delivery,[1] cell tracking,[2] cancer therapy,[3] magnetic resonance imaging[4,5] and heating elements for hyperthermia.[6] For these applications it is important to have total control of nanoparticle properties as well as high biocompatibility.[7]

SPIONS consist of iron oxide cores that can be guided to a specific target by an external magnetic field. They can be coated with different molecules to improve interactions with biological targets.[8] Surface modification of nanoparticles with hydrophilic polymers that have low toxicity and immunogenicity -such as polyethylene glycol (PEG) -reduces the interfacial energy in aqueous environments, which inhibits aggregation and contributes to nanoparticle formulation stability. As shown by Roberts et al,[9] low molecular weight chains of PEG (<400 Da) present toxicity as a result of the *in vivo* degradation by the alcohol dehydrogenase to toxic metabolites, and a lack of toxicity was observed for chains with more than 1000 Da. Moreover, the

Conflict of interest: The authors declare no conflict of interest.

This study was supported by grants from CNPq (Conselho Nacional de Desenvolvimento Científico e Tecnológico), CAPES (Coordenação de Aperfeiçoamento de Pessoal de Nível Superior) and FAPESC (Fundação de Amparo à Pesquisa de Santa Catarina) and is part of the doctoral studies of Adny Henrique Silva.

*Corresponding author.
E-mail addresses: tania.pasa@ufsc.br, taniabcp@gmail.com (T.B. Creczynski-Pasa).

http://dx.doi.org/10.1016/j.nano.2015.12.371
1549-9634/

stealth of the nanoparticle's surface with hydrophilic polymers can minimize unwanted opsonization and cellular recognition, giving them a long circulation time.[10,11]

The circulation time also depends on the hydrodynamic radii and superficial particles charge. The methoxy PEG (mPEG) presents advantages compared to the PEG (-OH terminal) because of the neutral charge and lower hydrodynamic radii, together with a reduced toxicity.[9] The size and surface modification of the nanoparticles lead to different responses in terms of cell interaction.[12] Particles with hydrodynamic diameter of less than 100 nm should escape from the reticuloendothelial system (RES), pass through the capillary systems of organs and tissues, and are thus more effective for drug delivery purposes.[8] Regarding the surface modification, several reports have demonstrated that the coating of nanoparticles protects them from the premature drugs release.[1,8]

From the magnetic point of view, the behavior of the SPIONS guarantees a null magnetization of nanoparticles at room temperature (RT), given their superparamagnetic properties, avoiding the formation of agglomerates, which would have drastic consequences for the exposed organisms. Moreover, the superparamagnetism allows a high susceptibility, with a strong response for an external magnetic field.

A variety of methods has been reported in the literature for the synthesis of magnetic nanoparticles with a controlled size and shape.[7] The nanoparticles evaluated in this work were prepared by thermal decomposition of organometallic precursor at high temperatures, resulting in samples of different systems with controlled size distribution and morphology.[13–18] The methodology used was similar to that described by Lima Jr. et al,[13] in which the final diameter of nanoparticles can be tailored by the synthesis temperature, the total synthesis time and the molar ratio between the metallic precursor and the surfactant. This synthesis procedure allows the production of nanoparticles with some desirable features, including controlled mean diameter, very narrow size dispersion and high crystallinity. The crystallinity leads to a magnetic system with optimized properties. However, the as-made nanoparticles are coated with oleic acid and consequently present a hydrophobic character, making necessary a post-synthesis procedure to decrease the hydrophobicity.[19]

In the present work, superparamagnetic iron-oxide nanoparticles in the size range of 20 nm and narrow dispersion were prepared. Hydrophilic nanoparticles were coated with a bi-layer consisting of oleic acid and PEG-phospholipid conjugates (mPEG), with distinct molecular mass of PEG (2000 g/mol, PEG2000, and 350 g/mol, PEG350). In order to characterize the biocompatibility of these formulations, a series of *in vitro* and *in vivo* assays were carried out. According to our results, the SPIONS coated with the distinct PEG conjugates presented different behavior in terms of cell uptake and toxicity, which is of great interest for future medical application.

Materials and methods

Nanoparticle synthesis and characterization

The nanoparticles were prepared by the decomposition of Iron (III) acetylacetonate (2.8 mMol) during 20 min in reflux condition, in the presence of oleic acid (15.7 mMol) and trioctylamine (91 mMol), with purities of 97, 99 and 98%, respectively (Aldrich, St. Louis, MO, USA). The reaction was carried out with magnetic stirring and N_2 flux (0.5 ml/min). The nanoparticles were precipitated by adding ethanol (97%) and by centrifugation (2000 × g, 10 min). The as-made nanoparticles presented hydrophobic character, which was changed to hydrophilic with a bi-layer consisting of the oleic acid and a conjugate of phopholipid-mPEG (polyethylene glycol), using mPEG of two molecular weight: 1,2-dioleoyl-*sn*-glycero-3-phosphoethanolamine-N-[methoxy(polyethylene glycol)-350] (ammonium salt) (99%); and 1,2-dioleoyl-*sn*-glycero-3-phosphoethanolamine-N-[methoxy(polyethylene glycol)-2000] (ammonium salt) (99%) from Avanti Lipids, Alabaster, AL, USA. The ratios of nanoparticle to conjugate were 1:2 *wt* and 1:2.2 *wt* for the mPEG2000 and mPEG350, respectively. Finally, the final samples were dispersed in water and labeled as SPION-PEG350 and SPION-PEG2000. SPION-PEG350 and SPION-PEG2000 were marked with the fluorescent agent FITC (Sigma-Aldrich, St. Louis, EUA). The aqueous nanoparticle solution were heated to 30 °C and placed at rest for 2 h at RT, protected from light. Finally, the SPIONS labeled with FITC were separated from the solution by magnetic separation, assuring that only the FITC linked to nanoparticles remains present.

Transmission electron microscopy (TEM) images of the as-made nanoparticles were obtained in a PHILIPS CM200 microscopy (*200 kV*). The X-ray patterns (XRD) were taken using a Philips PW346 diffractometer with the CuK_α radiation ($\lambda = 0.154186\ nm$). The Fourier transform infrared (FTIR) spectra were collected in a Frontier Perkin-Elmer spectrometer. The samples were conditioned in two ways, depending on the solvent used: a disk of potassium bromide with hydrophobic nanoparticles placed on it; the aqueous solution with hydrophobic particle was saturated with potassium bromide heated up until the solidification and the final powder was pressed. Hydrodynamic radius was measured by light scattering in a ZetaSizer 1000 (Malvern Instruments) with the nanoparticles dispersed in toluene or water depending on the coating.

Magnetization measurements (*M(T, 4 kA/m)* and *M(H, 300 K)*) were performed after fixing the particles in a polymeric matrix (Polyethylenimine, high molecular mass, Aldrich, St. Louis, MO, USA) in a SQUID (QUANTUM DESIGN) as well as in a vibrating sample (VSM, LakeShore) magnetometers. *M(T)* curves were measured in zero-field-cooling ($M_{ZFC}(T)$) and field-cooling ($M_{FC}(T)$) conditions in the temperature range indicated in the curve for each sample.

In vitro assays

Cell culture

Monkey kidney epithelium (Vero) and dog kidney fibroblasts (MDCK) were obtained from American Type Cell Culture (ATCC), and mouse embryonic fibroblast (NIH-3 T3) from Rio de Janeiro Cell Bank. The cells were cultured in DMEM supplemented with 10% heat-inactivated fetal bovine serum (both from Cultilab, São Paulo, Brazil), 100 UI/ml penicillin, 100 μg/ml streptomycin (Gibco, Grand Island, NY, USA) and 10 mM HEPES (Vetec, Rio de Janeiro, Brazil). Cells were

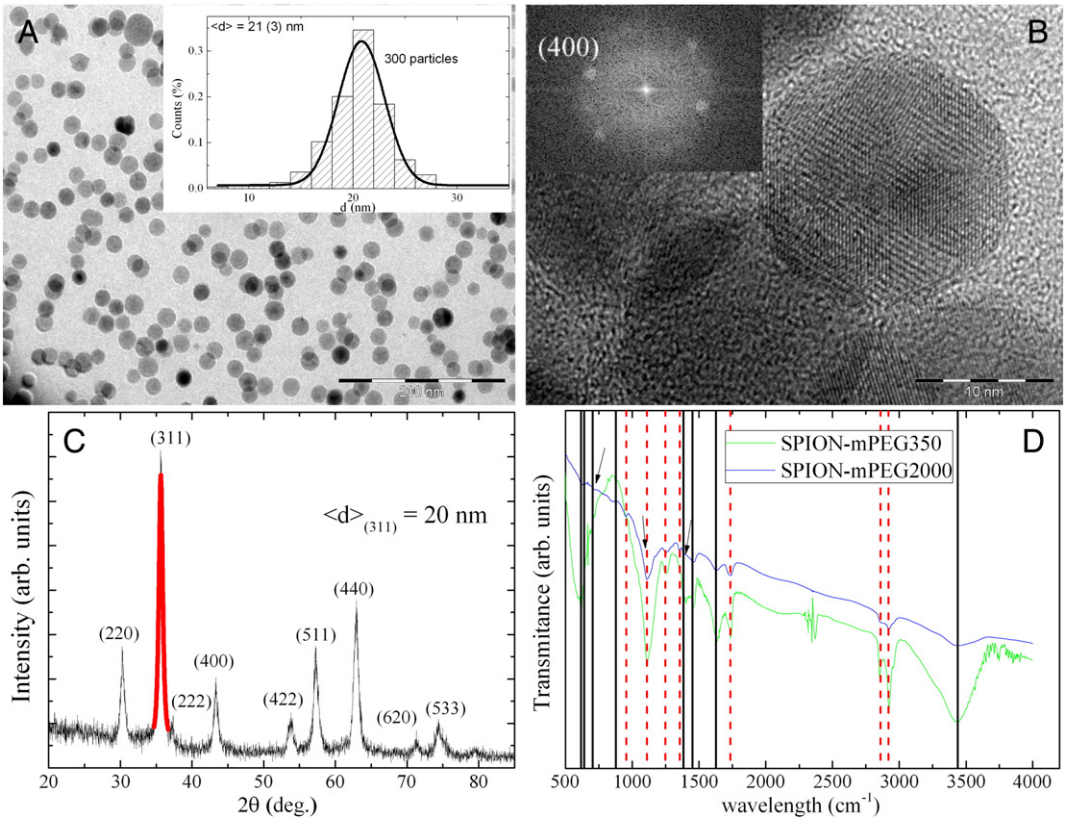

Figure 1. Representative TEM image, HRTEM image, XRD profile and FTIR spectra of nanoparticles. **(A)** Images of as-made nanoparticles with the histograms of diameters (inset) obtained by measuring more than 500 nanoparticles, fitted with a Gaussian distribution (< d > = 21 nm and sigma = 3 nm) (scale bar of 200 nm); **(B)** HRTEM image and the FTT (inset) and **(C)** XRD profile of the as-made sample (scale bar of 10 nm); **(D)** FTIR spectra of SPION-PEG350 and SPION-PEG2000 where the peaks corresponding to the oleic acid-magnetite (solid black lines) and PE-mPEG (dashed red lines) are indicated. The arrows are representative peaks, which are associated with functional groups of both organic components.

maintained at 37 °C in a 5% CO_2 humidified atmosphere and pH 7.4. Every 2–3 days, cells were passaged by removing 90% of the supernatant and replacing it with fresh medium.

In vitro cell viability assay

The cytotoxicity of nanoparticles was evaluated by MTT (Sigma-Aldrich, St. Louis, MO, USA).[20] Vero (1×10^4/0.2 ml), MDCK and NIH-3 T3 cells (2×10^4/0.2 ml) were incubated for 24 h with nanoparticle concentrations from 0 to 200 μg/ml, in triplicate, in 96-well microplates. A control using only nanoparticles and MTT was performed in parallel in order to exclude the possibility of MTT interference with nanoparticles (data not shown).

Cellular uptake of SPIONS by magnetization measurements

Vero, MDCK and NIH-3 T3 cells (1×10^6/3 ml) were incubated with 100 μg/ml of nanoparticles for 30 min, 24 h and 48 h. After treatment, the excess of SPIONS was removed by washing the cells three times with phosphate buffered saline (PBS). The cells were removed from the plates, re-suspended in PBS and cell uptake of SPIONS was measured by magnetization measurements.[21] *M(H,300 K)* curves for a known amount of cell were measured. The diamagnetic component is obtained from the linear fit of the high field region and the magnetization of the superparamagnetic component is obtained from the linear coefficient of the linear fit. The amount of the nanoparticles is determined by comparing this value with the magnetization of a known amount of nanoparticles. Four values were obtained from each magnetization curve, and the value used was the arithmetic mean.

Fluorescence imaging

The uptake of fluorescent-labeled SPIONS was investigated in Vero, MDCK and NIH-3 T3 cells using confocal microscopy (Spectral Leica TCS SP5 II, Wetzlar, Germany). Cells (2×10^5/2 ml) were incubated with 100 μg/ml of nanoparticles, for 24 h in 6-well plates containing glass coverslips. After that, cells were fixed with paraformaldehyde 3% (Sigma-Aldrich, St. Louis, MO, USA) for 15 min at 4 °C, washed three times with PBS and finally the actin filaments and nucleus were labeled with Phalloidin-633 and DAPI, respectively (Sigma-Aldrich, St. Louis, MO, USA). The coverslips were then mounted on microscopy slides using a Prolong Antifade kit (Invitrogen, Oregon, USA). The microscopy slides were kept protected from light at −20 °C until analysis. Confocal acquisitions were performed at a magnification of 40×, and the scale bars represent a size of 50 μm.

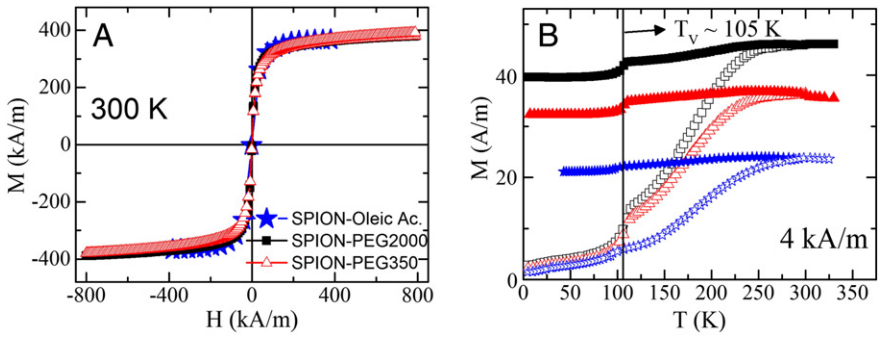

Figure 2. M(H) curves of the nanoparticles. M(H) curves of as-made nanoparticles (★), SPION-mPEG2000 (■) and SPION-mPEG350 (Δ) samples measured at 300 K **(A)**; M(T) curves of the three samples measured in ZFC (open symbols) and FC (solid symbols) modes **(B)**.

In situ atomic force microscopy (AFM) imaging of SPIONS-cell interaction

AFM images of live cells were obtained with a Bioscope Catalyst Atomic Force Microscope from Bruker ™. NIH-3 T3 (1×10^4/3 ml) cells were incubated with 100 μg/ml of nanoparticles for 30 min and immediately analyzed by AFM microscopy. For that, the plated cells were placed on the inverted microscope (Olympus IX81) coupled to the AFM that was used to select the cell to be imaged by AFM. The cantilever was positioned over the selected cell and images were obtained in fluid by tapping mode using Silicon nitride probes DNP-10 from Bruker ™ (cantilever D) at an average resonance of 12 kHz. The DNP probe used had a tip radius of 20–60 nm and was attached to a triangular cantilever of 200 μm in length with a spring constant of 0.06 N/m. Continuous time-lapse-images (in the height, amplitude and phase mode) of 1.5 × 1.5 μm (256 samples/line) were acquired for 12 min at the same surface location at a scan rate of 1.0 Hz.

In vivo acute toxicity studies

Animals and treatment

Swiss albino male mice, 6-8 weeks old, were maintained in accordance with the principles of Animal Care and procedures were approved by the Ethics Committee for Animals (01/2012). Prior to performing the experimental procedures, mice were matched for body weight (25 to 30 g). The animals were divided into four groups of ten mice each. The control group received only vehicle (saline) and treated groups received 12.5, 25 and 50 mg/kg/day of nanoparticles. The acute toxicity was performed according to the OECD-Guide (OECD-425/2008) and Guidance document, using cytotoxicity tests to estimate starting doses and treatment/monitoring time. According to OECD guideline, the doses used to investigate the toxicity of chemicals must be between 5 to 5000 mg/kg. Furthermore, as a new approach to assess acute toxicity, lethal doses should be avoided, monitoring the signs of toxicity as a toxicological approach.

The solutions were administered intravenously in a single dose in the tail vein and the individual body weights were recorded every two days until the last day the mice were kept alive. On the fourteenth day after the treatment the animals were anesthetized with ether, blood was collected from the retro orbital plexus, and the selected organs (liver, lung, kidney and heart) were removed. The removed organs were weighed for morphological analysis. All organs were fixed in 4% PBS-formaldehyde and processed as previously described.[22] Tissue sections were observed under a microscope at a magnification of 400×. Blood was used to evaluate hepatic, renal, and hematologic toxicity, as well as inflammatory markers.

Hepatic and renal function analysis

The blood samples were centrifuged at 400× g for 10 min at RT, and serum was separated to measure the alanine and aspartate aminotransferase activities (ALT and AST), total protein, albumin, urea and creatinine. For biochemical assays, commercially available kits (Labtest Diagnóstica SA, Lagoa Santa, MG, Brazil) were used (technical semi-automated biochemical analyzer Thermo Plate® Analyzer).

Hematological and inflammatory analysis

Hematological parameters such as red blood cell number (RBC), white blood cell number (WBC), lymphocyte and neutrophil counts were evaluated according to described elsewhere.[23] The serum content of hemoglobin, hematocrit, mean corpuscular hemoglobin (MCH), mean corpuscular volume (MCV) and mean corpuscular hemoglobin concentration (MCHC) were determined according to known method.[24] The cytokines TNF and IL-6 were measured in the serum of nanoparticle-treated mice by commercially available ELISA kits (BD OptEIA, San Diego, CA), according to the protocol described by the manufacturer.

Statistical analysis

The results of *in vitro* experiments were presented as means ± standard error of the mean (SEM) of triplicates from three-independent experiments and compared by one-way ANOVA, followed by Dunnet's test. The results of *in vivo* studies were presented as mean ± standard deviation (SD) (n = 6), and data were compared by one-way ANOVA followed by Bonferroni's test. $^*P < 0.05$ was taken as statistically significant.

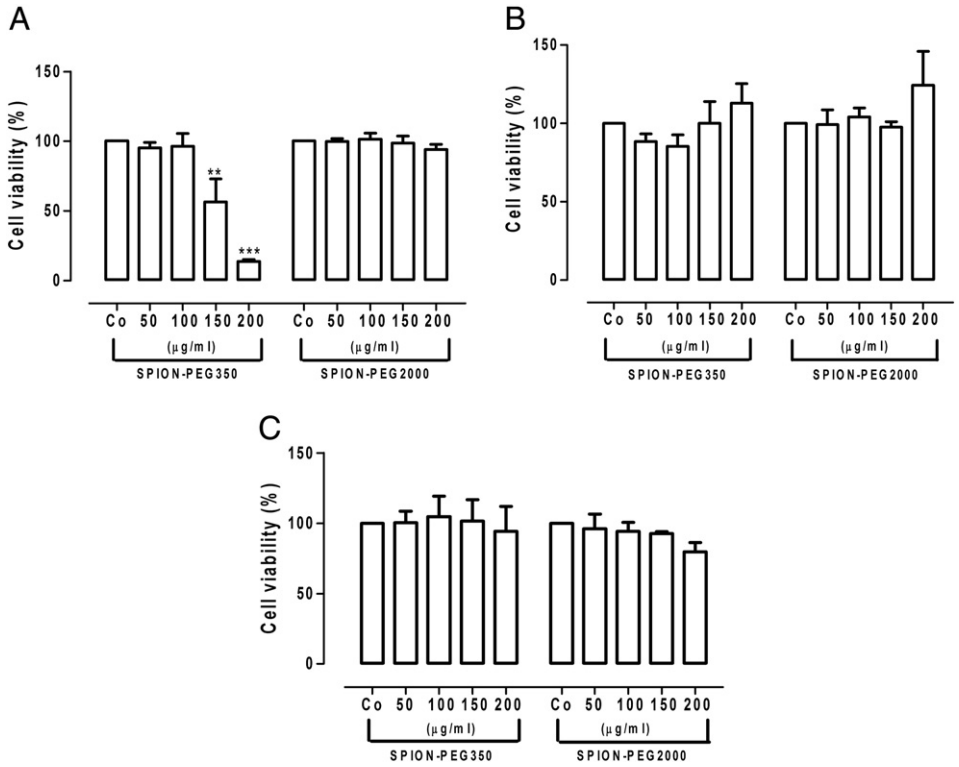

Figure 3. Analysis of cell viability after incubation with nanoparticles. Cell viability of Vero **(A)**, MDCK **(B)** and NIH-3 T3 **(C)** cells measured by MTT assay exposed to SPION-PEG350 and SPION-PEG2000 in function of the concentration (µg/ml). Cells were incubated with nanoparticles for 24 h. Optical density of untreated cells was taken as 100% of cell viability. *$P < 0.05$, **$P < 0.01$ and ***$P < 0.001$.

Results

Nanoparticle synthesis and characterization

Figure 1, *A* presents a representative TEM image of the as-made nanoparticles, which have a spherical-like shape with narrow size dispersion. The histogram of diameters presented in the inset of Figure 1, *A* was built up measuring more than 500 nanoparticles, and it is well fitted with a Gaussian distribution (solid line), taking $< d > =$ 21 nm and sigma = 3 nm. The HRTEM image (Figure 1, *B*) evidences the high crystallinity of the nanoparticles, which is very important for the magnetic properties of the system.

The FTIR spectra of SPION-mPEG350 and SPION-mPEG2000 (Figure 1, *D*), where the peaks indicated by the solid black lines and dashed red lines correspond to the oleic acid-iron oxide PE-mPEG conjugate, respectively. Some characteristic peaks were marked in the figure with arrows. These marked peaks are identified for the oleic acid as: peaks at 715 cm^{-1} – CH_2 rocking and 1384 cm^{-1} – CH_3[25]; and for mPEG as: 1105 cm^{-1} – alcohol.[26] These results confirm the formation of the bi-layer Oleic acid-PE-mPEG350 or Oleic acid-PE-mPEG2000 in the hydrophilic samples, which dictate the hydrophobicity of the as made nanoparticles. In fact, this property is easily observed when dispersing the samples in water or hexane.

The values of hydrodynamic diameter obtained for the SPIONS, SPION-PEG350 and SPION-PEG2000 were: 25 (5), 100 (20) and 80 (12) nm, respectively, the first one measured in toluene and the others in water. The formation of the bi-layer leads to an increment in the hydrodynamic diameter of the system. However, the hydrodynamic diameter measured for the pegylated nanoparticles is in the desirable range (<100 nm), a very useful size for biomedical applications.[27]

M(H) curves of oleic acid-, SPION-PEG350 and SPION-PEG2000 nanoparticles measured at RT presented no hysteresis, as expected for the superparamagnetic regime (Figure 2, *A*). All systems have high saturation magnetization (M_S) in comparison with other nanometric SPIONS at RT, about 400 kA/m; the M_S value of bulk material is about 512 kA/m.[28] M(T) curves of SPION-PEG350 and SPION-PEG2000 samples measured in ZFC and FC modes (Figure 2, *B*), which two main features are observed for all samples: first, an irreversibility temperature T_{Irr} at about 300 K (where the ZFC and FC M[T] curves have the same value), which corresponds to the highest blocking temperature of the system,[28] and a marked decrease in the magnetization in both modes at 100-120 K, which can be associated with the Verwey transition (Tv) characteristic of the Fe_3O_4 system with precise stoichiometry and high crystallinity.[29,30] An effective anisotropy constant of 5×10^5 erg/cm^3 is obtained from the mean blocking temperature (taken as the maximum in the energy barrier distribution calculated by $(1/T)d(M_{FC}\text{-}M_{ZFC})/dT$) and using the Néel model.[28] This is close to the value expected for the magneto crystalline anisotropy of the bulk magnetite.[28]

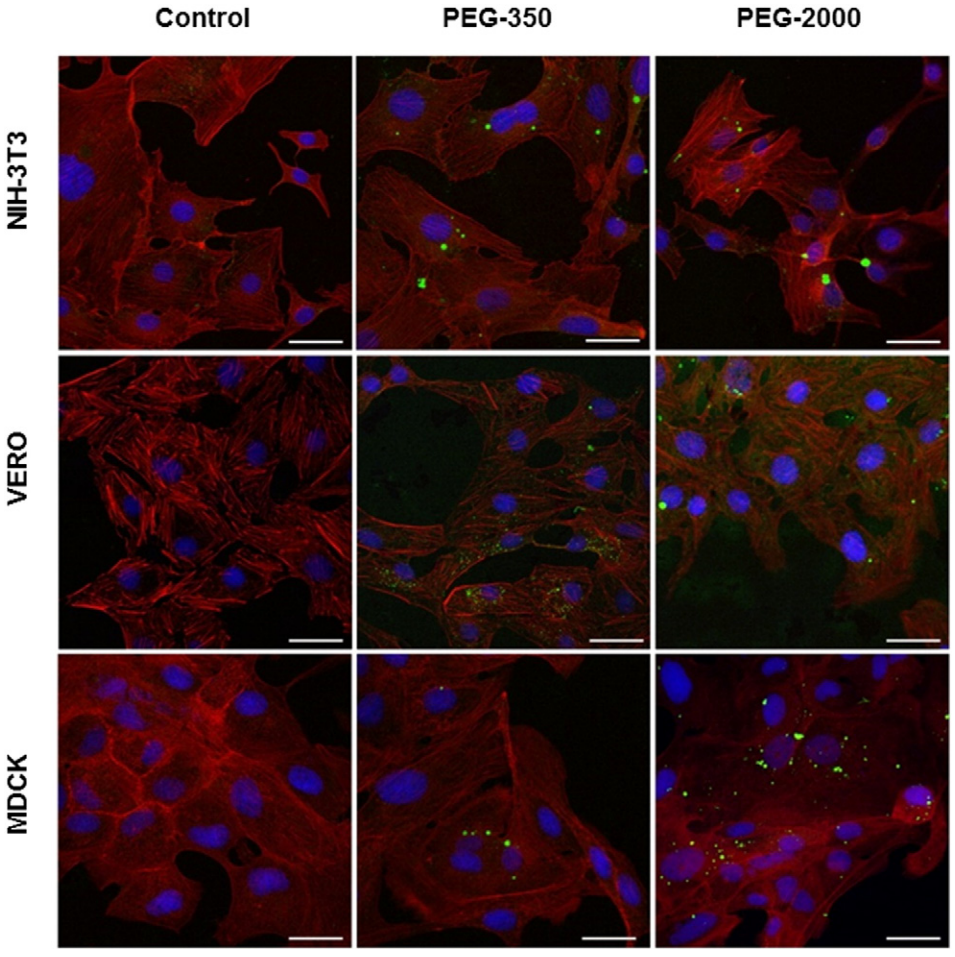

Figure 4. Cell uptake of nanoparticles analyzed by confocal microscopy. NIH3T3, Vero and MDCK cell lines were incubated for 24 h with SPION-PEG350-FITC or SPION-PEG2000-FITC as described in material and methods section. The cells were fixed and permeabilized and the actin filaments and nucleus were labeled with Phalloidin-633 and DAPI, respectively. The samples were mounted for laser confocal microscopy (LCM). Both SPIONS (PEG350-FITC and PEG2000-FITC) are showed in green, actin filaments in red and nuclei in blue. The merged images were obtained at a magnification of 40× and the scale bars represent a size of 50 μm.

Cell viability and SPIONS uptake

Figure 3, *A-C* presents the results of MTT assay of VERO, MDCK and NHI-3 T3 cell lineages, respectively, exposed to different concentrations of SPION-PEG2000 and SPION-PEG350 for 24 h. With regard to the cytotoxicity of SPION-PEG350, distinct behavior was observed depending on the cell lineage: cell viability of VERO cells was drastically reduced in concentrations higher than 100 μg/ml, while no reduction was observed in MDCK or NIH-3 T3 cells in concentrations as high as 200 μg/ml. For the SPION-PEG2000, even the higher concentration of 200 μg/ml did not induce cell toxicity, for all lineages studied, according to the MTT results.

According to the results of the confocal microscopy (Figure 4), uptake of SPION-PEG350-FITC and SPION-PEG2000-FITC were observed in all cell lines at the incubated time of 24 h. The nanoparticles' distribution was mainly cytoplasmic in all cell lines studied, and none of the SPIONS entered in the cell nuclei. SPION-PEG2000-FITC seems to be aggregated in all cell lines. Nevertheless, SPION-PEG350-FITC was less aggregated in Vero cells than in the other two cell lines.

In this study we used an independent quantification of SPION-PEG350 and SPION-PEG2000 cell uptake as a function of the exposition time using magnetization measurements. Figure 5 presents the results for the three cell lineages studied: VERO, MDCK and NIH-3 T3. These results clearly indicate a similar tendency to that observed in the images obtained by confocal microscopy: both SPIONS formulations were internalized by the three cell lines. However, higher uptake was found for the cells treated with SPION-PEG2000, with five-fold increase for Vero, two-fold increase for NIH-3 T3 and three-fold increase for MDCK cells after 24 h of incubation when compared with the SPION-PEG350 uptake. Interestingly, magnetization measurements provide quantitative results: 20-50 pg/cell for SPION-PEG2000 *vs* 10-12 pg/cell for SPION-PEG350 after 48 hours of incubation. In addition, for the SPION-PEG2000 there were significant differences between all the cell lines, with the greatest uptake in Vero cells. For the SPION-PEG350 the uptake in Vero and MDCK seems to be time dependent, which is not seen for NIH-3 T3, which showed similar uptake in the three times it was analyzed.

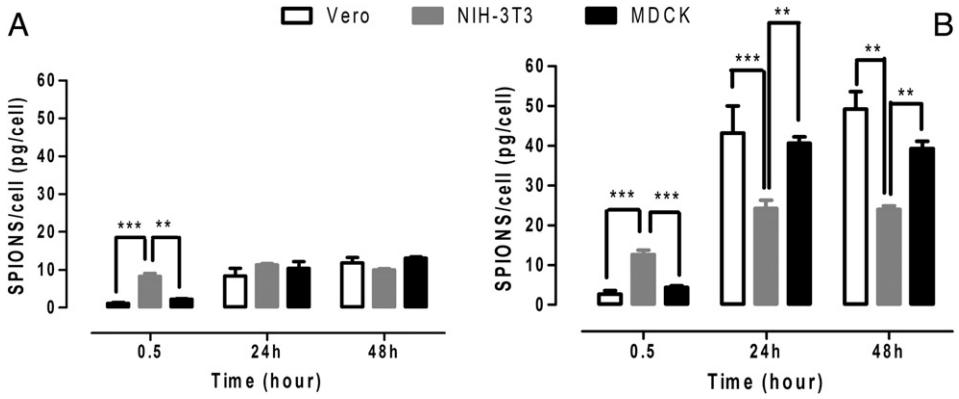

Figure 5. Nanoparticles uptake by the cell lines. Cell uptake of SPION-PEG350 **(A)** and SPION-PEG2000 **(B)** obtained from magnetic measurements as a function of the exposition time for the three studied cell lineages: VERO, NIH-3 T3 and MDCK3. Significant difference between $^{**}P < 0.01$ and $^{***}P < 0.001$.

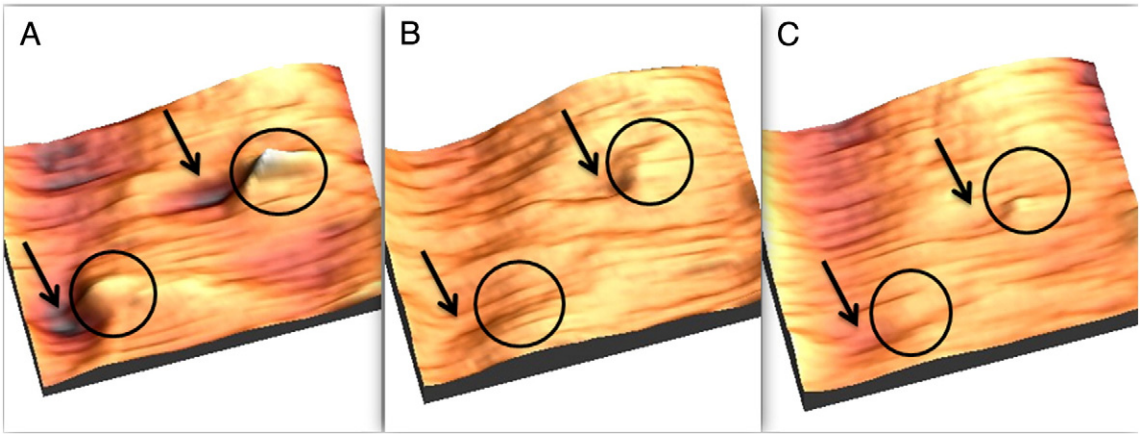

Figure 6. AFM images of nanoparticles uptake by the NIH-3 T3 cell line. Images of 1.5 × 1.5 μm showing changes on cell surface after incubation with SPION-PEG2000 for 0.5 h. The images were obtained after 4 **(A)**, 8 **(B)** and 12 **(C)** min finished the incubation time of cells with SPIONS. Arrows indicate the endocytic pits and circles indicate the presence of nanoparticles at the surface of cell.

Surface interaction between SPIONS and living cells was evaluated by AFM imaging in NIH-3 T3 (Figure 6). The figure shows the presence of nanoparticles on the surface of a cell, as evidenced by the circles and the formation of endocytic pits, indicated by the arrows (Figure 6, *A*). Images B and C were obtained after 8 and 12 min respectively, and show the disappearance of nanoparticle and endocytic pits closing, which suggests the internalization processes of SPIONS by the cells.

In vivo studies – acute toxicity

All animals tolerated the intravenous injections of nanoparticles, no animal died during the treatment and no significant differences were found in the mice's weight after treatment with nanoparticles (Figure S1 in supplementary material). Intravenous administration of nanoparticles did not significantly alter the organs' weight when compared with mice from the control group (see Table S1 in supplementary material).

The hematology profile of mice treated with SPION-PEG2000 is presented in Table 1. The results indicate that almost all hematological parameters were within normal ranges when compared with respective parameters found in the control group, with the exception of a significant increase in the basophil number and a significant decrease in the mononuclear cells.

Injection of SPION-PEG2000 caused no change in the serum cytokines IL-6 and TNF-α levels in mice, independently of the dose administrated, when compared with respective controls (Figure S2 in supplementary material).

The results of biochemical analysis are summarized in Table 2. According to the results, there was no significant change in ALT or AST enzymes as well as albumin and urea among mice treated with nanoparticles, independent of the nanoparticle concentration administered. However, the treatment with the highest concentration of SPION-PEG2000 induced a significant increase in total protein and significant decrease in creatinine. These results encouraged us to investigate the histology of the main organs looking for signs of injury. Hepatocyte vacuolation, inflammatory infiltrate and necrosis were detected in the liver of the animals treated with 12.5, 25 and 50 mg/kg of SPION-PEG2000, respectively. Moreover, assessment of kidney indicated areas of necrosis in animals treated with

Table 1
Hematological parameters of mice treated by intravenous route with different concentrations of SPION-PEG2000.

Parameters	Control	12.5 mg/Kg	25 mg/Kg	50 mg/Kg
Erythrocites (/mm^3)	7.900.000 ± 620	7.055.000 ± 435	6.713.000 ± 569	6.879.000 ± 410
Leukocytes (/mm^3)	9.191 ± 698	7.293 ± 629	7.216 ± 693	6.875 ± 767
VCM (fl)	63 ± 3	62 ± 2	58 ± 2	60 ± 3
HCM (pg)	21 ± 2	20.5 ± 1.5	19.5 ± 2.5	20 ± 2
CHCM (%)	32.5 ± 1.5	32.5 ± 2.5	32.5 ± 1.5	33 ± 1
Hemoglobin (g/dl)	15 ± 3	15 ± 2	13.5 ± 1	14.5 ± 1.5
Hematocrit (%)	45 ± 4	45 ± 1.3	40 ± 2	44 ± 2
Neutrophil (%)	24 ± 5	22 ± 6	39 ± 4	40 ± 5
Mononuclear (%)	74 ± 2	65 ± 10	46 ± 5**	42 ± 4**
Bastone (%)	–	–	4 ± 2	2 ± 1
Eosinophil (%)	–	–	–	–
Basophil (%)	2 ± 1	13 ± 2*	11 ± 3	16 ± 5**

* $P \leq 0.05$.
** $P \leq 0.01$.

Table 2
Biochemical parameters of mice treated by intravenous route with different concentrations of SPION-PEG2000.

Parameters	Control	12.5 mg/Kg	25 mg/Kg	50 mg/Kg
ALT (UI/l)	153 ± 7.3	170 ± 14	148 ± 11	149 ± 11
AST (UI/l)	111 ± 2	114 ± 12	104 ± 13	136 ± 4
Total proteins (g/dl)	5.2 ± 0.06	5.7 ± 0.1	5.9 ± 0.2	6 ± 0.3*
Albumin (g/dl)	2 ± 0.02	2.1 ± 0.1	1.9 ± 0.1	2.2 ± 0.1
Urea (mg/dl)	59 ± 4.2	57 ± 5.8	51 ± 1.8	57 ± 4.5
Creatinine (mg/dl)	0.5 ± 0.03	0.5 ± 0.01	0.5 ± 0.02	0.4 ± 0.01*

* $P \leq 0.05$.

12.5 and 25 mg/kg, respectively, as well as vacuolar congestion in animals treated with the highest concentration. Infiltrate inflammatory was also identified in lung of mice treated with 25 and 50 mg/kg of SPION-PEG2000. Cardiomyocytes presented intact intercalated discs and no inflammation signal was found, which indicate healthy tissue (Figure 7).

In order to improve the drugs circulation time when compared with other organic coating, such as DEXTRAN or PEI, liposomal encapsulated systems based on PEG-lipid conjugates have been used from a long time.[31,32] In addition, the methoxy in mPEG should increase the inert character of the PEG-phospholipid conjugate, also reducing the toxicity from the metabolism of the PEG molecule extremities OH groups. Therefore, the magnetic nanoparticles coated with the oleic acid – PE-mPEG groups developed in this work, should present a long circulation time, being very useful for example in magnetic-assisted drug delivery, using of an external magnetic gradient to improve the concentration of magnetic nanoparticles in a target tissue, in comparison with PEG and DEXTRAN coated nanoparticles.

Discussion

Our results indicate that the method used to synthetize magnetic nanoparticles allowed us to obtain "*high quality*" SPIONS coated with mPEG350 and mPEG2000: a system with controlled mean diameter, narrow sized distribution, high crystallinity as well as excellent and desirable magnetic properties.

Both SPIONS synthetized with different mPEG chain size were non-toxic *in vitro* up to the concentration of 100 μg/ml. Three different cell lines were used to better characterize the SPIONS as cytotoxic or not, since the response obtained with the *in vitro* assays can be directly related to the morphological and structural differences between the cells studied. Although the SPIONS studied here were prepared using the same method and had similar properties such as size and charge (almost neutral as consequence of the methoxy group), they are composed of a distinct PEG chain, which according to previous reports might significantly change distribution and toxicological responses.[33–36] The hypothesis proposed for the difference in the toxicity of SPION-PEG350 observed for Vero cells might be related to the properties of the cell line such as plasma membrane composition, but also to the PEG chain length, polymer chain architecture and interfacial PEG chain density,[37] since the same concentration of SPION-PEG2000 tested in the same cell line was not cytotoxic. However, the low toxicity of the SPION-PEG2000 for all lineages and the low toxicity of SPION-PEG350 for the NIH-3 T3 and MDCK lineages indicate a high degree of efficiency in the formation of methoxy ending-group in the polymeric chains.

The coatings might affect not only the viability of cells but also the SPIONS uptake, as well as general SPIONS–cell interaction.[38] Serum adsorption on the nanoparticle surface can determine the uptake of nanoparticles,[39] and increased PEG chain can decrease total protein adsorption. This could explain the highest uptake of SPION-PEG2000, since according to the results of confocal and magnetization measurement, the largest PEG chain size of this formulation seems to be essential to the nanoparticles' internalization, increasing at least two-fold the uptake rate according to the cell lineage. Even with the protein adsorption dictating the uptake, the interaction between PEG chain or methoxy group with cell surface may also determine the uptake rate.[40] Further studies must be performed to characterize the mechanisms related.

Within the past few years, AFM has been successfully used to study the morphology of nanoparticles and living cells. According to Spudich and Braunstain,[41] AFM enable the study of dynamics plasma membrane and identification of pit like structures in live cells, which was identified in NIH-3 T3 cells

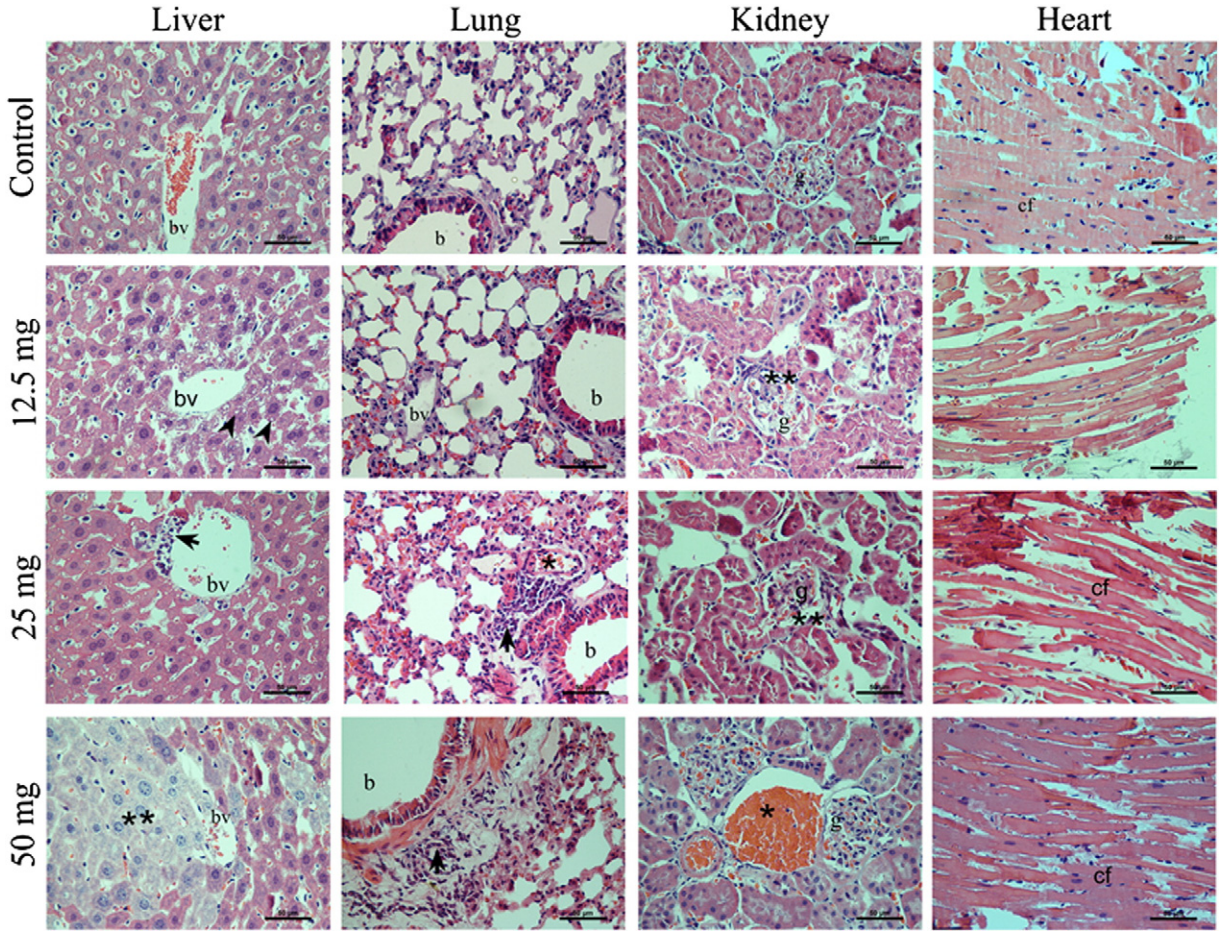

Figure 7. Histopathological analysis of organs after SPION-PEG2000 treatment. Vascular congestion (asterisk) and inflammatory infiltrate (arrow), typical signs of inflammation; hepatocyte vacuolation (arrowhead) and necrosis (double asterisk), typical signs of cell degeneration. Hematoxylin/Eosin stain. b, bronchioles; bv, blood vessel; cf, cardiac fiber; g, glomerulus. Scale bars represent a size of 50 μm.

after treatment with SPION-PEG2000. The endocytic pit formation was probably a result of SPION-PEG2000 attachment in cell surface, which was followed by their endocytosis, since nanoparticle disappeared after twelve minutes.

Furthermore, the behavior of SPION-PEG350 in Vero cells showing less aggregation could explain their toxicological effect in this cell line, since the small size of SPION-PEG350 provides an increased surface area which might increase their reactivity with cell macromolecules.[42] According to Rabolli et al,[43] properties such as size and surface area are frequently related to potential toxicity.

As SPIONS are likely candidates for *in vivo* medical application as a drug delivery system or in magnetic resonance images, it is essential to understand their behavior *in vivo*. The acute toxicity of SPION-PEG2000 was evaluated after single intravenous administration of three different doses of nanoparticles. SPION-PEG2000 formulation was chosen for *in vivo* evaluation according to results obtained *in vitro* in which (i) no toxicity was observed in all cell lineages, even with the higher concentration (up to 200 μg/ml); (ii) according to the PEG chain size; (iii) and according to the higher capability of SPION-PEG2000 to be internalized and accumulated inside the cell lineages studied.

As a particulate material, nanoparticles in contact with blood might react as a foreign body and consequently induce inflammatory response and hematological changes.[44] In addition, the degradation product from nanoparticle coating or even the core material might also trigger changes in hematologic parameters.[45] The basophil and mononuclear cells change might be associated with prolonged nanoparticle residence in systemic blood circulation. Similar behavior was observed after intravenous administration of PLA-PEG and PLGA-PEG nanoparticles, which remained in the systemic circulation for days, whereas PLA and PLGA nanoparticles are removed from the blood within a few minutes.[46] According to Nielsen,[47] an increase in basophil is a common response after some drugs' intravenous administration.

According to Hauck et al,[48] after nanoparticles leave the bloodstream and reach vital organs such as the kidney or liver, they might induce toxicity including inflammation, either by themselves or after the release of their constituents or metabolites. Inflammatory cells can trigger chronic inflammation, characterized by mononuclear cell infiltration and tissue destruction.[49] Results of histopathological evaluation showed inflammatory infiltrate, hepatocyte vacuolation and necrosis of

liver, kidney necrosis as well as inflammatory infiltration in lung. These results are in accordance with previously published works in which metallic nanoparticles, including iron oxide nanoparticles, induced liver, kidney and lung damage.[50-52,47] Furthermore, the increase in serum protein induced by SPION-PEG2000 has been correlated with liver damage as well as the decrease in creatinine has been correlated with kidney function, as pointed by Beeman et al[53] and Zhang et al.[54]

A limitation of the current study, which we can point, is that the adsorption, distribution and metabolism of SPION-PEG2000 as well as the possible oxidative stress involved in the toxicity mechanism of the SPIONS were not investigated. Also ammonia could be measured as a predictor of liver synthetic capacity as well as bilirubin and gamma glutamyltransferase (GGT), which are considered markers of cholestatic liver injury.[55] Nevertheless, these topics will be explored in further studies. However, these findings are very important for future nanoparticle application as drug delivery, cancer treatment and diagnosis, because the synthesis of "high quality" nanocarriers need to follow careful assessment of biocompatibility and safety to avoid toxicological unexpected events.

Acknowledgments

The authors wish to thank to Prof. Evelize Nazari, PhD and Cláudia A. C. Albuquerque, MSc from the Animal Reproduction and Development Laboratory at the Federal University of Santa Catarina (UFSC), for the histopathological evaluation.

Appendix A. Supplementary data

Supplementary data to this article can be found online at http://dx.doi.org/10.1016/j.nano.2015.12.371.

References

1. Guo S, Li D, Zhang L, Li J, Wang E. Monodisperse mesoporous superparamagnetic single-crystal magnetite nanoparticles for drug delivery. *Biomaterials* 2009;**30**:1881-9.
2. Rogers WJ, Meyer CH, Kramer CM. Technology insight: in vivo cell tracking by use of MRI. *Nat Clin Pract Cardiovasc Med* 2006;**3**:554-62.
3. Salata O. Applications of nanoparticles in biology and medicine. *J Nanobiotechnol* 2004;**2**:1-6.
4. Weissleder R, Bogdanov A, Neuwelt EA, Papisov M. Long-circulating iron oxides for MR imaging. *Adv Drug Deliv Rev* 1995;**16**:321-34.
5. Wang J, Huang Y, David AE, Chertok B, Zhang L, Yu F, et al. Magnetic nanoparticles for MRI of brain tumors. *Curr Pharm Biotechnol* 2012;**13**:2403-16.
6. Elsherbini AAM, Saber M, Aggag M, El-Shahawy A, Shokier HAA. Magnetic nanoparticle-induced hyperthermia treatment under magnetic resonance imaging. *Magn Reson Imaging* 2011;**29**:272-80.
7. Petcharoen K, Sirivat A. Synthesis and characterization of magnetite nanoparticles via the chemical co-precipitation method. *Mat Sci Eng B* 2012;**177**:421-7.
8. Mahmoudi M, Sant S, Wang B, Laurent S, Sen T. Superparamagnetic iron oxide nanoparticles (SPIONs): development, surface modification and applications in chemotherapy. *Adv Drug Deliv Rev* 2011;**63**:24-46.
9. Roberts MJ, Bentley MD, Harris JM. Chemistry for peptide and protein PEGylation. *Adv Drug Deliv Rev* 2002;**54**:459-76.
10. Wattendorf U, Merkle HP. PEGylation as a tool for the biomedical engineering of surface modified microparticles. *J Pharm Sci* 2008;**97**:4655-69.
11. Kohler N, Fryxell GE, Zhang M. A bifunctional poly(ethylene glycol) silane immobilized on metallic oxide-based nanoparticles for conjugation with cell targeting agents. *J Am Chem Soc* 2004;**126**:7206-11.
12. Wu X, Tan Y, Mao H, Zhang M. Toxic effects of iron oxide nanoparticles on human umbilical vein endothelial cells. *Int J Nanomedicine* 2010;**5**:385-99.
13. Lima EJ, De Biasi E, Vasquez Mansilla M, Saleta ME, Effenberg F, Rossi LM, et al. Surface effects in the magnetic properties of crystalline 3 nm ferrite nanoparticles chemically synthesized. *J Appl Phys* 2010;**108**:103919, http://dx.doi.org/10.1063/1.3514585 [10p].
14. Sun S, Zeng H. Size-controlled synthesis of magnetite nanoparticles. *J Am Chem Soc* 2002;**124**:8204-5.
15. Sun S, Zeng H, Robinson DB, Raoux S, Rice PM, Wang SX, et al. Monodisperse MFe_2O_4 (M = Fe, Co, Mn) nanoparticles. *J Am Chem Soc* 2004;**126**:273-9.
16. Khandhar AP, Ferguson RM, Simon JA, Krishnan KM. Tailored magnetic nanoparticles for optimizing magnetic fluid hyperthermia. *J Biomed Mater Res A* 2012;**100**:728-37.
17. Vargas JM, Zysler RD. Tailoring the size in colloidal iron oxide magnetic nanoparticles. *Nanotechnology* 2005;**16**(2):1464-76.
18. Kwon SG, Hyeon T. Formation mechanisms of uniform nanocrystals via hot-injection and heat-up methods. *Small* 2011;**7**:2685-702.
19. Lan Q, Liu C, Yang F, Liu S, Xu J, Sun D. Synthesis of bilayer oleic acid-coated Fe_3O_4 nanoparticles and their application in pH-responsive Pickering emulsions. *J Colloid Interface Sci* 2007;**310**:260-9.
20. Mosmann T. Rapid colorimetric assay for cellular growth and survival: application to proliferation and cytotoxicity assays. *J Immunol Methods* 1983;**65**:55-63.
21. Zysler RD, Lima Jr E, Vasquez Mansilla M, Troiani HE, Mojica Pisciotti ML, Gurman P, et al. A new quantitative method to determine the uptake of SPIONs in animal tissue and its application to determine the quantity of nanoparticles in the liver and lung of Balb-c mice exposed to the SPIONs. *J Biomed Nanotechnol* 2013;**9**:142-5.
22. Silva AH, Locatelli C, Filippin-Monteiro FB, Zanetti-Ramos BG, Conte A, Creczynski-Pasa TB. Solid lipid nanoparticles induced hematological changes and inflammatory response in mice. *Nanotoxicology* 2013;**8**:212-9.
23. Garg DK, Goyal RN. Haematological and hepatotoxic effects of silken styles of corn in albino rats. *J Appl Toxicol* 1992;**12**:359-63.
24. Pari L, Murugavel P. Role of diallyl tetrasulfide in ameliorating the cadmium induced biochemical changes in rats. *Environ Toxicol Pharmacol* 2005;**20**:493-500.
25. Wu N, Fu L, Su M, Aslam M, Chun Wong K, Dravid VP. Interaction of fatty acid monolayers with cobalt nanoparticles. *Nano Lett* 2004;**4**:383-6.
26. Castillo PM, de la Mata M, M. Casula F, Sánchez-Alcázar JA, Zaderenko AP. PEGylated versus non-PEGylated magnetic nanoparticles as camptothecin delivery system. *Beilstein J Nanotechnol* 2014;**5**:1312-9.
27. Ujiie K, Kanayama N, Asai K, Kishimoto M, Ohara Y, Akashi Y, et al. Preparation of highly dispersible and tumor-accumulative, iron oxide nanoparticles multi-point anchoring of PEG-b-poly(4-vinylbenzylphosphonate) improves performance significantly. *Colloids Surf B* 2011;**88**:771-8.
28. Cullity BD, Graham CD. *Introduction to magnetic materials*. Wiley-IEEE Press; 2009.
29. Aragon R, Gehring PM, Shapiro SM. Stoichiometry, percolation, and Verwey ordering in magnetite. *Phys Rev Lett* 1993;**70**:1635-8.
30. Seo H, Ogata M, Fukuyama H. Aspects of the Verwey transition in magnetite. *Phys Rev B* 2002;**65**:085107, http://dx.doi.org/10.1103/PhysRevB.65.085107 [8p].

31. Gabizon A, Goren D, Cohen R, Barenholz Y. Development of liposomal anthracyclines: from basics to clinical applications. *J Control Release* 1998;**53**:275-9.
32. Working PK, Newman MS, Sullivan T, Yarrington J. Reduction of the cardiotoxicity of doxorubicin in rabbits and dogs by encapsulation in long-circulating, pegylated liposomes. *J Pharmacol Exp Ther* 1999;**289**:1128-33.
33. Bartneck M, Peters FM, Warzecha KT, Bienert M, van Bloois L, Trautwein C, et al. Liposomal encapsulation of dexamethasone modulates cytotoxicity, inflammatory cytokine response, and migratory properties of primary human macrophages. *Nanomedicine* 2014;**10**:1209-20.
34. Cruz LJ, Tacken PJ, Fokkink R, Figdor CG. The influence of PEG chain length and targeting moiety on antibody-mediated delivery of nanoparticle vaccines to human dendritic cells. *Biomaterials* 2011;**32**:6791-803.
35. Mao S, Neu M, Germershaus O, Merkel O, Sitterberg J, Bakowsky U, et al. Influence of polyethylene glycol chain length on the physicochemical and biological properties of poly(ethylene imine)-graft-poly(ethylene glycol) block copolymer/SiRNA polyplexes. *Bioconjug Chem* 2006;**17**:1209-18.
36. Khargharia S, Kizzire K, Ericson MD, Baumhover NJ, Rice KG. PEG length and chemical linkage controls polyacridine peptide DNA polyplex pharmacokinetics, biodistribution, metabolic stability and in vivo gene expression. *J Control Release* 2013;**170**:325-33.
37. Malmsten M, Emoto K, Van Alstine JM. Effect of chain density on inhibition of protein adsorption by poly(ethylene glycol) based coatings. *J Colloid Interface Sci* 1998;**202**:507-17.
38. Mahmoudi M, Simchi A, Milani AS, Stroeve P. Cell toxicity of superparamagnetic iron oxide nanoparticles. *J Colloid Interface Sci* 2009;**336**:510-8.
39. Lesniak A, Fenaroli F, Monopoli MP, Aberg C, Dawson KA, Salvati A. Effects of the presence or absence of a protein corona on silica nanoparticle uptake and impact on cells. *ACS Nano* 2012;**6**:5845-57.
40. Unsworth LD, Sheardown H, Brash JL. Protein-resistant poly(ethylene oxide)-grafted surfaces: chain density-dependent multiple mechanisms of action. *Langmuir* 2008;**24**:1924-9.
41. Spudich A, Braunstein D. Large secretory structures at the cell surface imaged with scanning force microscopy. *Proc Natl Acad Sci U S A* 1995;**92**:6976-80.
42. Luque-Garcia JL, Sanchez-Díaz R, Lopez-Heras I, Camara C, Martin P. Bioanalytical strategies for in-vitro and in-vivo evaluation of the toxicity induced by metallic nanoparticles. *Trends Anal Chem* 2013;**43**:254-68.
43. Rabolli V, Thomassen LCJ, Uwambayinema F, Martens JA, Lison D. The cytotoxic activity of amorphous silica nanoparticles is mainly influenced by surface area and not by aggregation. *Toxicol Lett* 2011;**206**:197-203.
44. Nel A, Xia T, Madler L, Li N. Toxic potential of materials at the nanolevel. *Science* 2006;**311**:622-7.
45. Karmakar R, Bhattacharya R, Chatterjee M. Biochemical, haematological and histopathological study in relation to time-related cadmium-induced hepatotoxicity in mice. *Biometals* 2000;**13**:231-9.
46. Zambaux MF, Faivre-Fiorina B, Bonneau F, Marchal S, Merlin JL, Dellacherie E, et al. Involvement of neutrophilic granulocytes in the uptake of biodegradable non-stealth and stealth nanoparticles in guinea pig. *Biomaterials* 2000;**21**:975-80.
47. Nielsen FH. Silicon deprivation does not significantly modify the acute white blood cell response but does modify tissue mineral distribution response to an endotoxin challenge. *Biol Trace Elem Res* 2010;**135**:45-55.
48. Hauck TS, Anderson RE, Fischer HC, Newbigging S, Chan WC. In vivo quantum-dot toxicity assessment. *Small* 2010;**6**:138-44.
49. Gil A. Polyunsaturated fatty acids and inflammatory diseases. *Biomed Pharmacother* 2002;**56**:388-96.
50. Chen J, Dong X, Zhao J, Tang G. In vivo acute toxicity of titanium dioxide nanoparticles to mice after intraperitoneal injection. *J Appl Toxicol* 2009;**29**:330-7.
51. Gui S, Zhang Z, Zheng L, Cui Y, Liu X, Li N, et al. Molecular mechanism of kidney injury of mice caused by exposure to titanium dioxide nanoparticles. *J Hazard Mater* 2011;**195**:365-70.
52. Wu W, Chen B, Cheng J, Wang J, Xu W, Liu L, et al. Biocompatibility of Fe3O4/DNR magnetic nanoparticles in the treatment of hematologic malignancies. *Int J Nanomedicine* 2010;**5**:1079-84.
53. Bheeman D, Cheerothsahajan S, Sugumaran S, Mathan S, Mathan R, Dakshanamurthy S, et al. Indium titanium oxide nanoparticles induced hepatic damage: hepatoprotective role of novel 2-Imino-4-methyl-1, 2-Dihydropyrimido [5, 4C] Quinoline-5(6H)-one. *Adv Toxicol* 2014;**2014**:641813, http://dx.doi.org/10.1155/2014/641813 [7p].
54. Zhang X-D, Wu D, Shen X, Liu P-X, Yang N, Zhao B, et al. Size-dependent in vivo toxicity of PEG-coated gold nanoparticles. *Int J Nanomedicine* 2011;**6**:2071-81.
55. Ramaiah SK. A toxicologist guide to the diagnostic interpretation of hepatic biochemical parameters. *Food Chem Toxicol* 2007;**45**:1551-7.